Dynamic Masking Application Examples in Two-Phase Flow PIV Measurements

F. Gökhan Ergin[1] *, Jimmy Olofsson[2], Bo B. Watz[3], Nicolai Fog Gade-Nielsen[3]

1: Microfluidics Product Manager, Dantec Dynamics, DENMARK
2: LIF Systems Product Manager, Dantec Dynamics, DENMARK
3: Software Development Engineer, Dantec Dynamics, DENMARK
*Corresponding author: gokhan.ergin@dantecdynamics.com

Keywords: Phase-separated PIV processing, dynamic masking, histogram thresholding, phase boundary detection, flame front detection, rigid object stabilization

ABSTRACT

Dynamic masking and phase-separated PIV processing are powerful analysis tools during two-phase flow field diagnostics. This paper aims to summarize an overview of several dynamic masking techniques used in ten different application examples, and to make recommendations on masking strategy in different applications. The examples cover a wide range of applications: all possible two-phase flow combinations, micrometer to decimeter scales, flows with and without temperature gradients can be found among the examples. The application examples include: droplet formation in micro-channels, mixing of two liquids in microscale using magnetic forces, bubbly flow in water, combustion in a low-swirl lifted flame, a vibrating airplane model in a wind tunnel, two puller-type micro swimmers with one pulling breaststrokes and the other using its flagellum, dolphin kick of a human swimmer, spinning micro-rafts on the air-water interface, and a breaking wave experiment in a wave tank.

1. Introduction

Dynamic masking and phase-separated PIV processing have become standard routines during two-phase flow field diagnostics. Different dynamic masking strategies have been reported in the literature, which can be grouped under three categories (Brücker 2000): (i) during image recording using additional optical systems and components to record one of the phases (optical phase separation, OPS) (ii) during image processing before PIV processing (digital phase separation, DPS) and (iii) post-PIV analysis using differentiators in the cross-correlation function (post-phase separation, PPS). Furthermore, the digital phase separation techniques can be grouped under four categories: (ii-a) size based discrimination (SBD), (ii-b) histogram thresholding (HT), (ii-c) phase boundary detection (PBD), and (ii-d) rigid object stabilization (ROS) techniques. In challenging cases, dynamic masks are often more successful if both optical and digital phase separation are used. This paper aims to summarize an overview of dynamic masking techniques used in ten different application examples and to make recommendations

on masking strategy in different situations. The examples cover a wide range of applications: all possible two-phase flow combinations, micrometer to decimeter scales, and flows with and without temperature gradients can be found among the examples. A summary of the application examples are listed in Table 1, where HT, PBD and ROS techniques are used.

Experiment	Phases	Scale	Equipment	Masking Strategy	Seeding	Illumination	Frequency
Droplet formation	Liq-Liq	µm	TR µPIV	DPS (**HT**)	1.1µm	Continuous broadband	20 000 Hz
Flagellum swimmer	Sol-Liq	µm	TR µPIV	DPS (**HT**)	1.0 µm	Green pulsed LED	12.5 Hz
Dolphin kick	Sol-Liq	dm	TR PIV	DPS (**HT**)	100 µm	TR PIV laser	250 Hz
Spinning micro-rafts	Sol-Liq	µm	TR Stereo µPIV	DPS (**HT**)	5 µm	TR PIV laser	300 Hz
Breaking wave	Gas-Liq	dm	TR PIV	DPS (**HT**)	10µm	TR PIV laser	96 Hz
Magnetic micromixer	Liq-Liq	µm	µPIV	DPS(**PBD**)	1.0 µm	Green pulsed LED	4 Hz
Bubbly flow	Gas-Liq	cm	TR PIV	OPS+**PBD**	20µm-50µm	PIV Laser + red LED	400 Hz
Lifted flame	Gas-Gas	cm	TR PIV + TR OH LIF	OPS+**PBD**	1µm	TR PIV and TR tunable dye laser	4 000 Hz
Airplane model	Sol-Gas	mm	Long-range µPIV	DPS (**ROS**)	1.0 µm	PIV laser	10 Hz
Breaststroke swimmer	Sol-Liq	mm	Long-range TR µPIV	DPS (**ROS**)	2.0 µm	Infrared CW laser	2 000 Hz

Tab. 1 An overview of the application examples with different dynamic masking strategies.

The motivation behind dynamic masking is to perform phase-separated PIV measurements and thereby reduce the measurement uncertainty significantly along the phase boundaries. This is crucial, since often important fluid dynamics phenomena occur close to a phase boundary, i.e. surface of a swimmer, flying object, combustion zone or a mixing layer. Therefore, detection and separation of phases using dynamic masking provides more accurate PIV measurements and thereby a better understanding of fluid phenomena near phase boundaries.

The application examples include: droplet formation in micro-channels (Fig. 1), a puller-type micro swimmer using a flagellum (Fig. 2), dolphin kick of a human swimmer (Fig. 3), spinning micro-rafts on the air-water interface (Fig. 4), a breaking wave experiment in a wave tank (Fig. 5), mixing of two liquids in microscale using magnetic forces (Fig. 6), combustion in a low-swirl lifted flame (Fig. 7), bubbly flow in water (Fig. 8), a vibrating airplane model in a wind tunnel (Fig. 9), and a micro swimmer pulling double-breaststrokes (Fig. 10).

2. Histogram Thresholding (HT) Examples

HT-based dynamic masking relies on the pixel intensity differences (bimodal histograms) between the phases for phase discrimination. The phase to be masked (can be solid, liquid or gas) should have a certain pixel value distribution that is lower or higher than a certain threshold. Once such a threshold is selected, the pixel values lower than the threshold can be set to zero, and the rest to 1. The new image ensemble is then called the mask ensemble, and masking is performed by a simple image multiplication at each time step of the ensemble. Selecting a threshold level in combination with some other image pre-processing functions (low-pass filters, morphology filters etc.) allows one to generate a dynamic mask that follows the phase or the object in the image ensemble. In the following five examples, we demonstrate the successful application of HT-based dynamic masking, at the same time highlighting some unwanted local artifacts observed in the field of view (FoV).

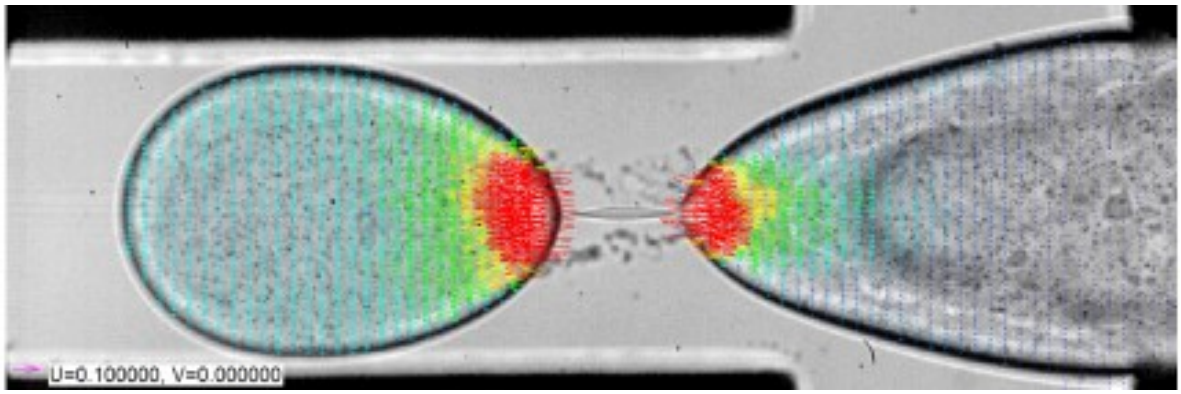

Fig. 1 Snapshot of the flow field at the rupture instance during the droplet break-up experiment performed in a microchannel. (from Carrier et al. 2015). Colors indicate velocity magnitude, max velocity 270 mm/s. Histogram thresholding based dynamic mask is able to follow morphological changes during droplet formation. (Collaboration: Université de Lorraine, CNRS)

HT-based dynamic masks are quite popular because they are relatively simple to apply and are quite powerful in applications where the phase to be masked has a complex shape and undergoing morphological changes (merging of bubbles, rupturing of droplets etc). Fig. 1 shows

an example of an HT-based dynamic mask applied in a micro-droplet formation experiment at the rupture instance. In order to capture the rupture event, the MicroPIV experiment was performed with single-frame image acquisition at 20 000 fps. A movie of this experiment is available in Ref. M1. As can be seen in the movie, the droplet goes through growth, necking, rupture and recoil phases where its shape, size, and morphology changes and this can be tracked successfully by the dynamic mask. Further details can be found in Carrier et al. (2015).

The second example on HT-based dynamic masking is the masking of a puller-type microscopic swimmer, where E. Gracilis (Fig. 2a) is meandering through water by pulling strokes using its anterior flagellum, and changing direction by rotating, bending and stretching its body (Fig. 2e-f). HT-based mask is generated (Fig. 2c) after background subtraction (Fig. 2b) and the mask is applied using a number of image processing functions (Fig. 2d). Although HT masking is very successful in following flexible objects that are changing shape (bending, stretching etc.), some unwanted artifacts can be observed. For example in this case, excessive use of the morphology filters (erosions and dilations) makes the mask size larger than the actual object size close to the edges of the FoV (compare top of Fig. 2e-f). Further details can be found in Ergin (2015, 2017).

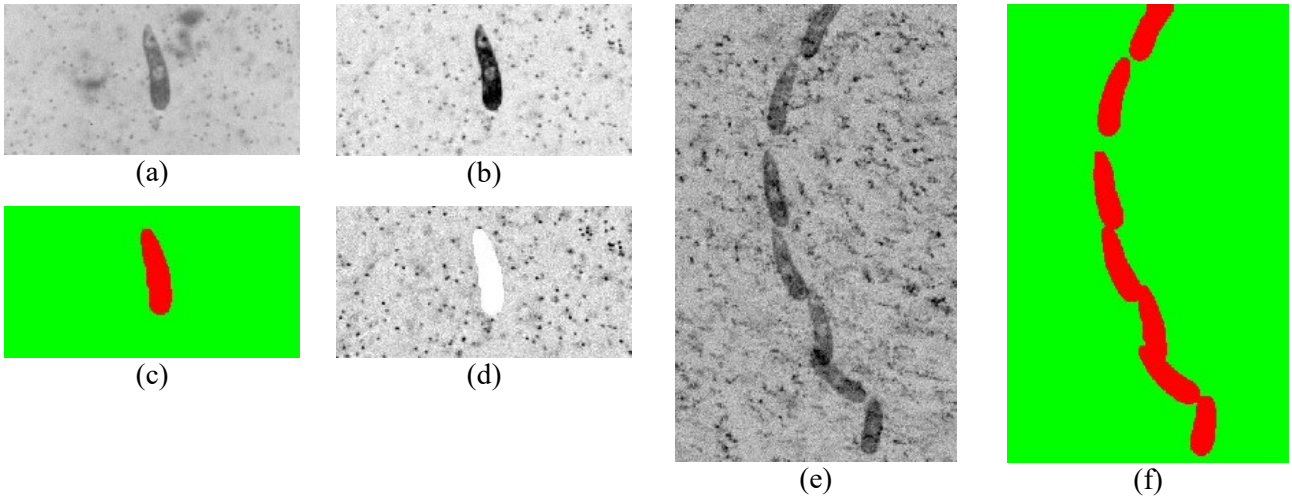

Fig. 2 (a, b, c, d) Snapshot of a microorganism (E. Gracilis) swimming horizontally in water at t=1.92 s. (a) Raw image (b) after pixel inversion and background subtraction (c) HT-based dynamic masking (d) particle image after image masking. (e, f) Quality of dynamic masking: (e) Recorded position (f) dynamic mask of E. Gracilis every 0.96s. From Ergin (2015).

HT-based dynamic masking can be used successfully for macroscopic swimmers as well as for microscopic swimmers. Fig. 3 shows the flow field around a human swimmer's feet while performing a dolphin kick. A movie of this experiment is available in Ref. M2. The experiment is performed in a swimming pool, using a time-resolved PIV system with a powerful laser where

the human subject was wearing proper laser protection equipment. The masking strategy reveals the large trailing vortex caused by the kick, and the downwash of the water above the foot sole. However, due to the focused laser light sheet, high-intensity reflections were observed around the toes, where the fluid phase was registered as a mask, and therefore in the immediate vicinity of the toes flow field information could not be obtained. On the contrary, some regions on the leg and heels were not masked due to a low pixel value found in these regions. Further details on undulatory swimming can be found in Hochstein et al. (2012).

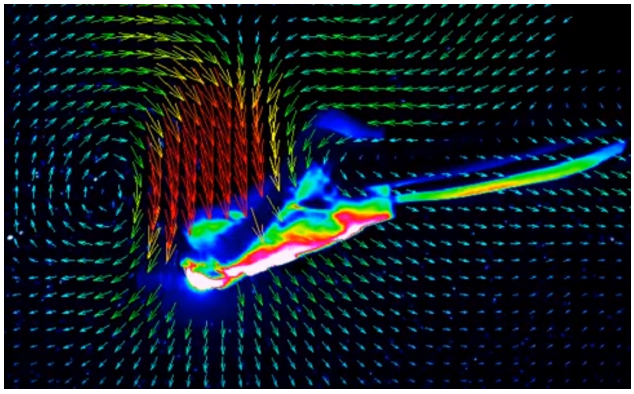

Fig. 3 Flow field around the feet of a human swimmer performing a "Dolphin kick" in a swimming pool. One side effect of the HT- based dynamic masking is that vectors appear on the swimmers left foot in the dark regions, and no vectors are found around the toes of the right foot due to strong reflections in the fluid phase. (Collaboration: Friedrich-Schiller-Universität, Jena)

HT-based dynamic masking can be applied to multiple-camera systems (f. ex. Stereoscopic PIV) as well as single camera systems. Fig. 4 shows the application of an HT-based masking strategy in a stereoscopic MicroPIV experiment using two cameras. The experiment intends to capture the three-dimensional motion of the free surface while a pair of micro-rafts are spinning in the clockwise direction. Although the generated dynamic masks are circular like the rafts, the masked areas in the Stereoscopic velocity fields are not circular in certain time instances. This can be explained by the lack of seeding near the rafts (red circles in Fig. 4a): Due to the high rotation speed (2500 rpm) used in this experiment, the seeding particles are pushed away from the rafts due to centrifugal forces. The lack of seeding in a high velocity region introduces a higher uncertainty in the cross-correlation based displacement estimation in the immediate vicinity of the rafts in individual camera views. As a result of this, the Stereoscopic construction accuracy is lower, and these vectors are discarded by the algorithm. In short, although the raw images of the rafts and the dynamic masks generated from these are quite round and symmetric (Fig. 4a), the resulting flow field information may not be due to low seeding density (Fig. 4b). Further details can be found in Ergin et al. (2017a).

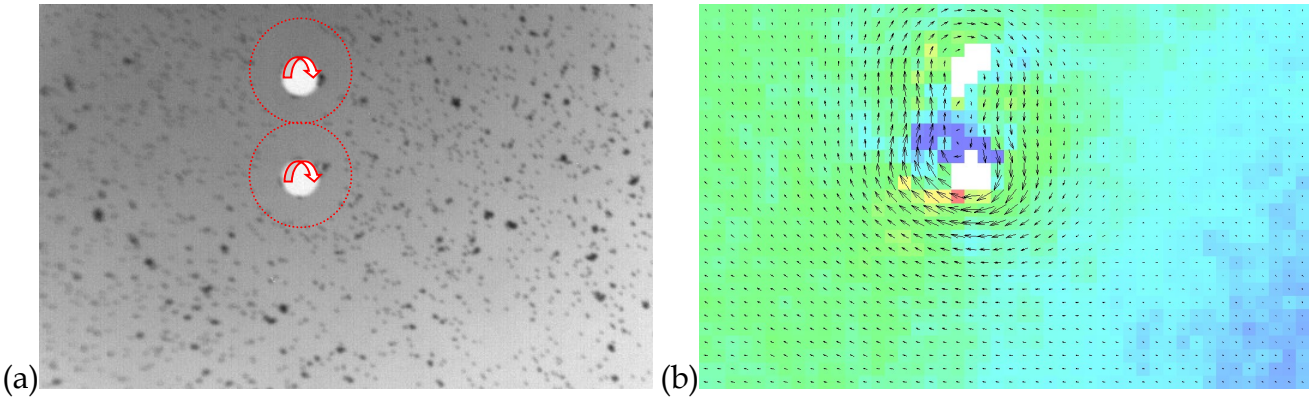

Fig. 4 (a) Raw image of the spinning micro-rafts. Red arrows indicate rotation direction; red dashed circles show the boundary for low seeding concentration (b) Stereoscopic PIV results at the same instant where colors indicate out of plane velocity component and white color indicates where vectors fall in the circular masked areas. From Ergin et al. (2017a) (Collaboration: Max Planck Institute).

Another successful example for HT-based dynamic masking in variable seeding density is from a wave tank experiment. In this case the measurement area is illuminated from below and due to expanding light sheet propagating upwards, the lower left and lower right corners of the FoV is not sufficiently illuminated. Additionally, the bubbles and droplets over the free surface and the image of the free surface is not desirable (Fig. 5a). Following a background subtraction, difference of Gaussian filters, opening and closing filters a dynamic mask ensemble was generated to mask everything except the seeded area (Fig. 5b). The flow field is obtained using a PIV/PTV algorithm where the low seeding areas can be seen (Fig. 5c). Further details can be found in Vested et al. (2018).

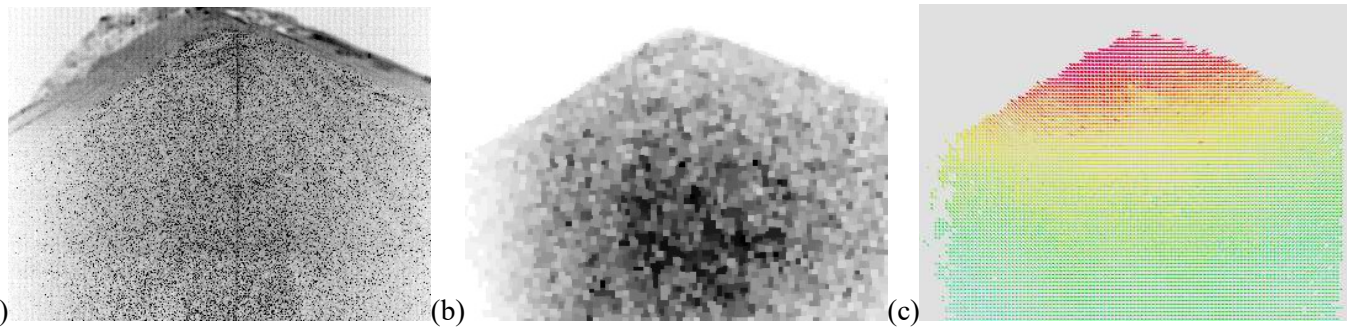

Fig. 5 Snapshot from the breaking wave experiment in a wave tank. (a) Inverted raw particle image of the breaking wave traveling to the left. (b) Result of image pre-processing just before histogram thresholding is applied (c) PIV/PTV results displayed on a regular grid where colors indicate velocity magnitude (Collaboration: Technical University of Denmark).

3. Phase Boundary Detection (PBD) Examples

As discussed in the previous section, HT-based masking strategies are quite powerful in generating dynamic masks, but some unwanted artifacts can be observed on the boundaries due to reflections, excessive use of certain image processing functions and/or due to lack of seeding

in stereoscopic reconstruction. One solution is to use phase boundary detection (PBD), a novel, hybrid dynamic masking technique reported recently (Ergin et al. 2017b), where both pixel intensities and/or intensity gradients are used for phase discrimination. In the following three examples, the successful application of PBD-based dynamic masking is presented.

(a) (b)

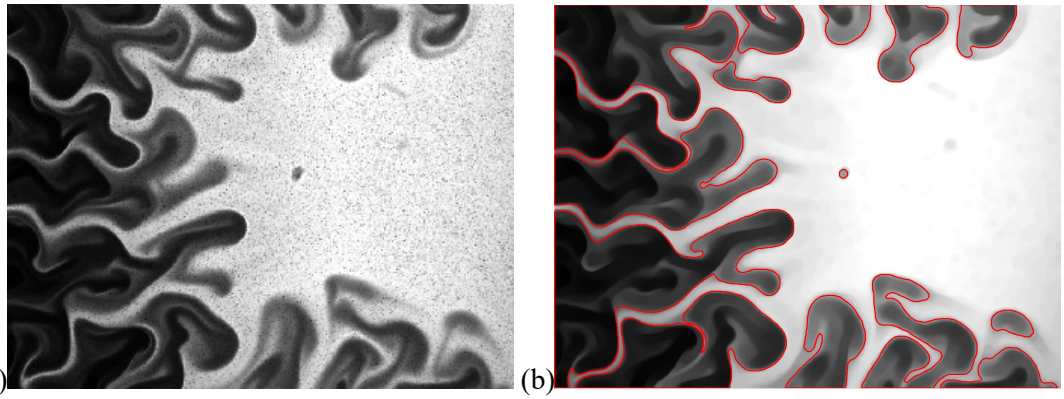

Fig. 6 (a) Snapshot from the magnetic micromixer experiment reported in Ergin et al. (2014) with magnetic fluid (dark phase) and water (bright phase). (b) The detected phase boundary (red line). Phase boundary detection technique is powerful in detecting phases with a large spectrum of local pixel value gradients. (Collaboration: University of Latvia)

Pixel intensity differences exist frequently in the liquid-liquid mixing applications. One example is taken from a magnetic micromixer (Fig. 6), where there is a clear difference between the optical absorption rates of liquid water (brighter phase) and magnetic fluid (darker phase), in this case, water doped with magnetic nanoparticles. In this experiment (reported in Ergin et al. 2014 among others) the two liquids are forced into each other using magnetic forces. A movie of this experiment is available in Ref. M3. A shadow imaging technique was used and the difference in the optical absorption rates was sufficient to create an overall distinction between the phases (OPS was not necessary). However, since this is a mixing experiment, the intensity gradients were found to lie in a wide range (very shallow to very steep gradients), and often it was difficult to decide where to place the phase boundary (red line in Fig. 6b) on a shallow intensity gradient. Therefore, for the magnetic micromixer experiment shown in Fig. 6a, only the pixel intensities in a local and finite bounding box were used for phase discrimination by applying Otsu thresholding. This strategy is not only a systematic way to place the phase boundary, but also a more powerful one compared to the simpler HT-based dynamic masking. Further details can be found in Ergin et al. 2017b.

In other cases, pixel intensity gradients should be considered in addition to the pixel intensities during phase discrimination. Fig. 7 shows the phase separation of raw images (Fig. 7a-b) and the resulting flow field (Fig. 7c) across a turbulent, premixed lifted flame. The experiments were

performed using a time-resolved PIV and OH-LIF system triggered simultaneously. Since the OH distribution was used for the generation of the dynamic mask, this application example is combining OPS and DPS. In the combustion process, the OH radical is produced very close to the reaction zone and diminishes gradually with increasing distance from the flame front. In other words, very steep gradients of the OH radical marks the flame front and the phase boundary and shallower gradients indicate the regions where OH reacts with other molecules to form the combustion products. For this reason, the pixel intensity gradients in the OH image (not shown) are used for phase discrimination in conjunction with the pixel intensity differences. Immediately apparent from the raw images is the substantial difference in the seeding densities of the fuel phase (Fig. 7a) and the combustion products (Fig. 7b) across the flame front. This is due to the sudden heat release in the reaction zone which results in an expansion in the combustion products phase. The PBD based dynamic masking together with OPS lends itself to better phase discrimination and to phase-separated PIV measurements (Fig. 7c) where the measurement accuracy is improved significantly compared to mixed-phase PIV analysis. Further details can be found in Ergin et al. (2017b).

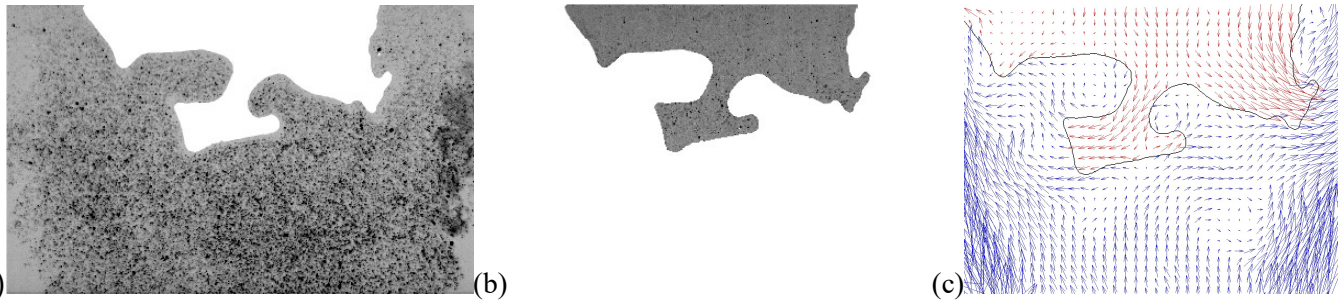

Fig. 7 Application of phase boundary detection (PBD) based dynamic masking used in combination with optical phase separation (OPS) using an OH-LIF system in a swirling lifted flame experiment. (a) 1st frame of the fuel phase of the raw particle image pair, (b) same for the combustion products phase (c) Close-up of the phase-separated PIV measurement results at the same instant. Red vectors are in the products phase, blue vectors are in the fuel phase, and the continuous black line depicts the flame front. From Ergin et al. (2017b) (Collaboration: Lund University)

Like the HT-based techniques, the PBD-based dynamic masking techniques can handle morphological changes (merging and separating) quite well. In the next example, the PBD-based masking technique is applied to a flow field with rising bubbles (Fig. 8a) where two bubbles are merging later during the process (Fig. 8b). This is the second example where PBD is used in combination with OPS, because a separate shadow illumination/recording system is used. However, because of the choice of the wavelengths, some cross-talk was observed in the images. This can be observed in the particle images within the large bubble in the middle in Fig. 8a. These are either particles located behind the bubble refracting through the bubble, or in front of the bubble, reflecting from the bubble surface. Additionally, the bubbles are transparent and

appear as hollow rings in the raw images and a simple HT-based masking cannot be used here. In fact, this example is the most challenging example in terms of the number of challenges involved: (i) arbitrary shape and direction, (ii) phase to be masked is hollow, (iii) morphological changes (merging and separation), (iv) cross-talk between the two optical systems, and (v) intensity differences in the particle images due to shadows cast by the bubbles. Despite the challenges, image pre-processing and PBD-based dynamic masking provides very good results (Fig. 8)

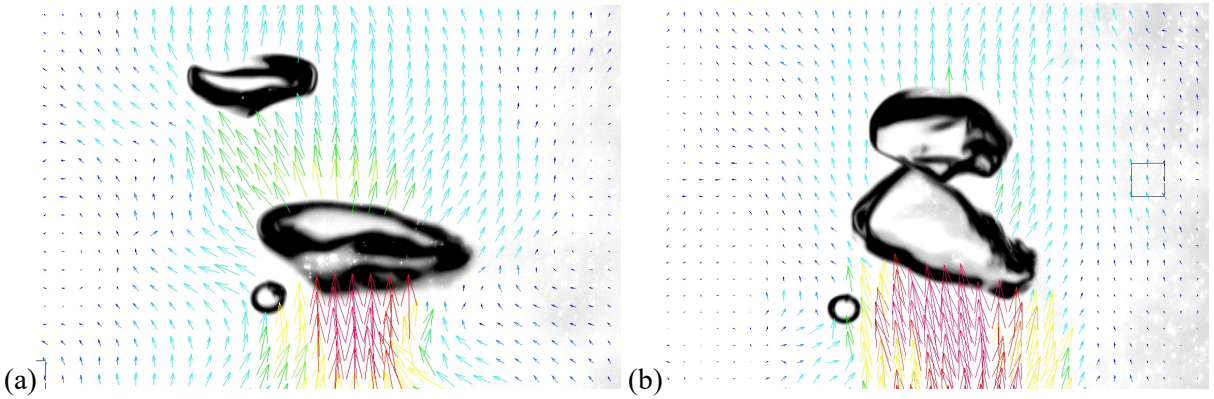

Fig. 8 (a) Close up of flow field around 3 bubbles rising in water at t=8ms in a bubbly flow setup. (b) Same 3 bubbles at t=73ms. Phase boundary detection based dynamic masking is able to detect morphological changes such as bubbles merging or separating. Colors indicate velocity magnitude.

4. Rigid Object Stabilization (ROS) Examples

So far we have provided examples where the phase or object to be masked is changing shape or undergoing morphological changes, which is the case in many experiments. In other cases the object to be masked could be rigid, and simply translating and rotating within the FoV. In the next two examples, we discuss how dynamic masks can be produced in these situations. The basic idea is changing from a global coordinate system to an object-fixed coordinate system.

The first example is concerning boundary layer measurements of an airplane model in a wind tunnel (Fig. 9a) where a conventional 15Hz two-frame PIV acquisition mode is used. Due to aerodynamic forces, the model was observed to be moving a few pixels to a different position (Fig. 9b) from one acquisition to the next (i.e. from one pulse pair to the next), but seemed stationary within each pulse pair, thanks to the short pulse separation. If the aim is to perform unmasked PIV analysis, the movement of the model does not create any complications for individual flow fields. However, the accuracy gets worse when one wants to perform f. ex. statistical or modal analysis simply because computed velocity vectors lie in a different position with respect to the object. If the objective is to perform masked PIV analysis, or subsequent statistical or modal information is required, then the solid object must be first stabilized in the

FoV, before applying a static masking strategy. In this particular case, the solid object was stabilized by first extracting a rough shape of the object from, say, the first image, and correlating this sub-image to the full images of the ensemble. This results in the displacement of the object from one acquisition to the next (Fig. 9b) which can be corrected for in the next step by shifting the original images by the negative amount of each displacement. Once the object is stabilized in the FoV, and static masking is performed; the vector statistics results are much more accurate in the boundary layer compared to a similar analysis without ROS (Fig. 9c). Please note that the static masking performed after object stabilization is actually dynamic masking performed on the original images.

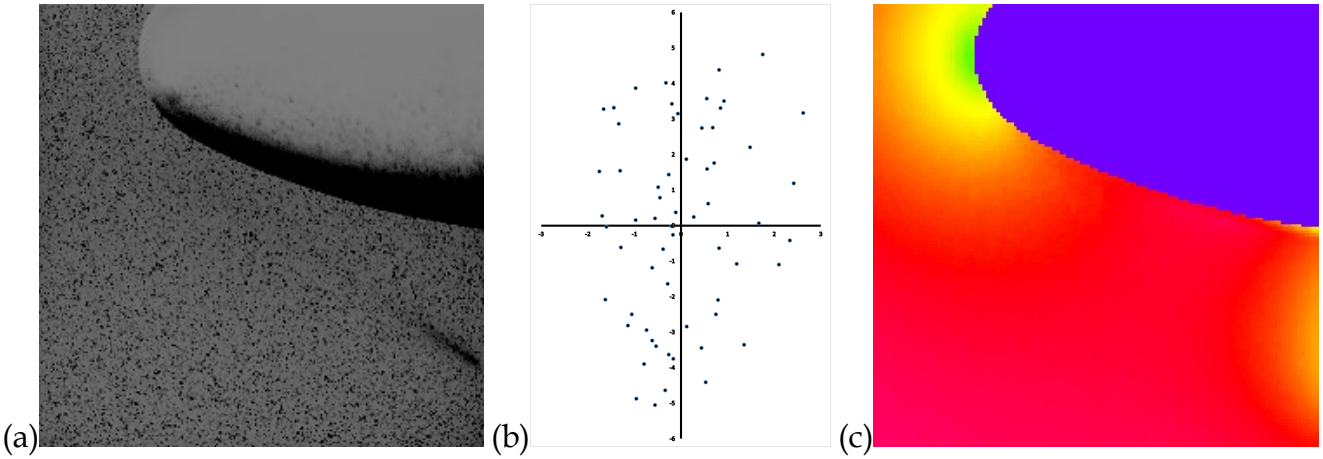

Fig. 9 Application of rigid object stabilization (ROS) based dynamic masking in a boundary layer flow around a model airplane in a wind tunnel. (a) Typical raw particle image where some surface features are visible on the airplane nose. From Ergin and Alemdaroğlu (2013). (b) Position of the airplane as it is moving around a few pixels from one acquisition to the next due to aerodynamic forces. (c) Mean of the horizontal velocity component, U (average of 61 vector maps) shown together with the used mask (purple)

The final dynamic masking example is the flow field measurements around a sub-mm sized marine organism while performing breast-strokes (Fig. 10a). In a long-distance MicroPIV experiment performed in the Technical University of Denmark, an individual Acartia Tonsa was captured while swimming against the gravitational field in a relatively straight trajectory (Ergin et al. 2015). In this acquisition A. Tonsa has performed three cycles of double-power strokes followed by a recovery stroke. The ROS is performed in a very similar fashion as described in the previous example: First a sub-image of the object is extracted from the first image of the example, then this was cross-correlated within the images of the entire ensemble and a region of interest (RoI) is extracted around the peak of the cross-correlation function (Fig. 10b). After performing ROS, applying a static mask and performing phase locked-averaging the flow field around A. Tonsa was obtained more accurately compared to earlier results (Fig. 10c). Further details can be found in Ergin et al. (2015) and Ergin (2017).

(a) 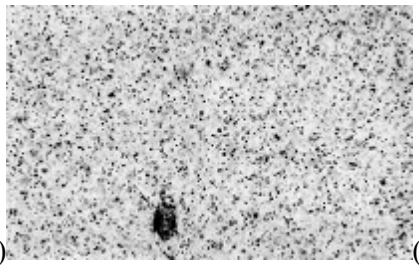 (b) 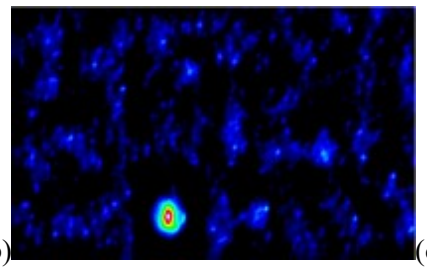 (c) 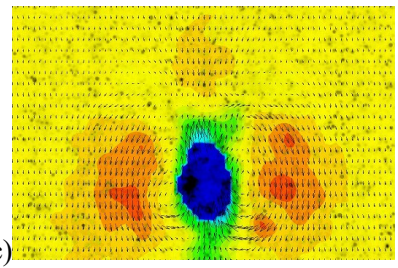

Fig. 10 Application of rigid object stabilization (ROS) based dynamic masking in a biological flow around A. Tonsa, swimming upwards in a water tank (a) First frame of the raw particle image ensemble where some seeding particles stuck on the swimmer are visible (b) Cross-correlation function of the organism with the 1st frame. (c) Flow field during the second power stroke shown together with the used mask (dark blue). Colors indicate velocity magnitude. From Ergin et al. (2015). (Collaboration: Technical University of Denmark)

5. Suggestions and Conclusions

Several dynamic masking strategies used in ten different application examples are presented. Some conclusions / recommendations can be made based on the foregoing discussion and based on the experience of the authors:

1. Most likely there is no magic masking strategy that works equally well for all the applications, and the masking strategy should be selected case by case.
2. Always prefer OPS in combination with DPS whenever possible.
3. Think about the OPS-based masking strategy already during the planning stage of the experiment, as f. ex. choice of correct illumination wavelength can make things much easier.
4. Use HT-based or PBD-based masking strategies if the masked phase or object has arbitrary shape and direction, or going through morphological changes (such as merging and separation)
5. HT-based dynamic masking may be the easiest strategy for certain cases, where a single thresholding operation can be sufficient for image segmentation. In other cases one may have to perform some image pre-processing to bring the image ensemble to a state ready for pixel-value thresholding.
6. Prefer the relatively simpler HT-based masking strategy for quick checks and preliminary results, and choose PBD-based masking strategies for more challenging situations and/or for more accurate results.
7. Start with an ROS-based masking strategy if the object to be masked is rigid. ROS-based masking strategies have the added advantage of measuring the velocity and accelerations of the rigid object that is to be masked.

6. Acknowledgements

The authors are indebted to several individuals for providing the raw image ensembles for dynamic masking and subsequent PIV analysis performed at Dantec Dynamics:
Denis Funfschilling (Fig. 1), Stefan Hochstein (Fig. 3), Ahmet Tabak and Wendong Wang (Fig. 4), Malene Vested (Fig. 5), Kaspars Erglis and Andrejs Cebers (Fig. 6), Per Petersson (Fig. 7), Zhang Yao (Fig. 8), and Navish Wadhwa (Fig. 10). Furthermore, the authors wish to thank Giovanni Noselli for providing the culture for Euglena Gracilis (Fig. 2).

7. Author Contributions

FGE: Definition, development and validation of HT, PBD, ROS techniques, preparation of setup and image acquisition of airplane model and flagellum swimmer experiment, image processing and dynamic masking for all application examples, abstract preparation, presentation preparation, manuscript preparation. **JO**: PBD definition and development, data acquisition and processing for the lifted flame experiment. **BW**: ROS development in DynamicStudio, image processing for magnetic micromixer, and airplane model experiments. **NGN**: PBD development in DynamicStudio, data processing for lifted flame experiment. All authors reviewed the manuscript.

8. References

- Brücker Ch (2000) PIV in two-phase flows. von Karman Institute for Fluid Dynamics, lecture series 2000–01
- Carrier O, Ergin FG, Li HZ, Watz BB & Funfschilling D (2015) Time-resolved mixing & flow-field measurements during droplet formation in a flow-focusing junction. J. Micromech. Microeng. 15 084014
- Ergin FG and Alemdaroğlu N (2013) Long-distance MicroPIV measurements of a commercial aircraft model at low Reynolds number. Proc. 7th Ankara International Aerospace Conference, Ankara, Turkey, AIAC-2013-013
- Ergin FG, Watz BB, Erglis K and Cebers A (2014) Modal analysis of magnetic microconvection. Magnetohydrodynamics Vol. 50 (2014), No. 4, pp. 339–352
- Ergin FG (2015) Flow field measurements during microorganism locomotion using MicroPIV and dynamic masking. Proc. 11th Int. Symp. on PIV, Santa Barbara, California, September 14-16, 2015

- Ergin FG, Watz BB and Wadhwa N (2015) Pixel-accurate dynamic masking and flow measurements around small breaststroke-swimmers using long-distance MicroPIV. Proc. 11th Int. Symp. on PIV, Santa Barbara, California, September 14-16, 2015
- Ergin FG. (2017) Dynamic masking techniques for particle image velocimetry. J. of Thermal Science and Technology,Vol 37, 2, pp. 61-74. ISSN 1300-3615.
- Ergin FG, Tabak AF, Wang W, Sitti M (2017a) Time-resolved measurements of the free surface motion due to spinning micro-rafts using Stereo MicroPIV. Proc. 12th International Symposium on Particle Image Velocimetery June 2017, Pusan, Korea
- Ergin FG, Olofsson J and Gade-Nielsen NF (2017b) Phase separated PIV Measurements Using Phase Boundary Detection. Proc. 12th International Symposium on Particle Image Velocimetry June 2017, Pusan, Korea
- Hochstein S, Pacholak S, Brücker C and Blickhan, R (2012) Experimental and numerical investigation of the unsteady flow around a human underwater undulating swimmer. In: C. Tropea & H. Bleckmann (Eds.) Nature-Inspired Fluid Mechanics, Notes on Numerical Fluid Mechanics and Multidisciplinary Design, 119, 293-308.
- Vested MH, Ergin FG, Carstensen S, and Christensen ED (2018) High-resolution planar two-component PTV measurements in a breaking wave. Proc. to 19th Int. Symp. on App. of Laser and Imaging Tech. to Fluid Mechanics, July 2018, Lisbon, Portugal.
- M1: https://www.dantecdynamics.com/microfluidics-category/time-resolved-velocity-measurements-of-droplet-formation-in-a-flow-focusing-junction
- M2: https://www.dantecdynamics.com/hydraulics-hydrodynamics-category/piv-measurements-during-the-dolphin-kick-of-a-human-swimmer
- M3: https://www.dantecdynamics.com/microfluidics-category/modal-analysis-in-a-micromixer